nature medicine

SUPPLEMENTARY INFORMATION

https://doi.org/10.1038/s41591-018-0263-8

In the format provided by the authors and unedited.

The molecular landscape of glioma in patients with Neurofibromatosis 1

Fulvio D'Angelo[1,2,41], Michele Ceccarelli[2,3,41], Tala[1], Luciano Garofano[1,2], Jing Zhang[1], Véronique Frattini[1], Francesca P. Caruso[2,3], Genevieve Lewis[1], Kristin D. Alfaro[4], Luc Bauchet[5], Giulia Berzero[6], David Cachia[7,8], Mario Cangiano[2], Laurent Capelle[9], John de Groot[10], Francesco DiMeco[11,12,13], François Ducray[14], Walid Farah[15], Gaetano Finocchiaro[16], Stéphane Goutagny[17], Carlos Kamiya-Matsuoka[10], Cinzia Lavarino[18], Hugues Loiseau[19], Véronique Lorgis[20], Carlo E. Marras[21], Ian McCutcheon[10], Do-Hyun Nam[22,23], Susanna Ronchi[6], Veronica Saletti[24], Romuald Seizeur[25], John Slopis[10], Mariona Suñol[26], Fanny Vandenbos[27], Pascale Varlet[28,29], Dominique Vidaud[30], Colin Watts[31], Viviane Tabar[32], David E. Reuss[33,34], Seung-Ki Kim[35], David Meyronet[36], Karima Mokhtari[6], Hector Salvador[37], Krishna P. Bhat[10], Marica Eoli[16], Marc Sanson[6], Anna Lasorella[1,38,39,42*] and Antonio Iavarone[1,39,40,42*]

[1]Institute for Cancer Genetics, Columbia University Medical Center, New York, NY, USA. [2]BIOGEM Istituto di Ricerche Genetiche 'G. Salvatore', Ariano Irpino, Italy. [3]Department of Science and Technology, Università degli Studi del Sannio, Benevento, Italy. [4]The University of Texas M.D. Anderson Cancer Center John Mendelsohn Faculty Center (FC7.3025) – Neuro-Oncology – Unit 0431, Houston, TX, USA. [5]Department of Neurosurgery, Gui de Chauliac Hospital, Montpellier University Medical Center, Montpellier, France. [6]Sorbonne Universités UPMC Université Paris 06, UMR S 1127, Inserm U 1127, CNRS UMR 7225, ICM, APHP, Paris, France. [7]Department of Neuro-Oncology, Medical University of South Carolina, Charleston, SC, USA. [8]Department of Neurosurgery, Medical University of South Carolina, Charleston, SC, USA. [9]AP-HP, Hôpital de la Pitié-Salpêtrière, Service de Neurochirurgie, Paris, France. [10]The University of Texas M.D. Anderson Cancer Center, Houston, TX, USA. [11]Department of Neurological Surgery, Carlo Besta Neurological Institute, Milan, Italy. [12]Department of Pathophysiology and Transplantation, University of Milan, Milan, Italy. [13]Hunterian Brain Tumor Research Laboratory CRB2 2M41, Baltimore, MD, USA. [14]Service de Neuro-Oncologie, Hospices Civils de Lyon, Université Claude Bernard Lyon 1, Department of Cancer Cell Plasticity, Cancer Research Center of Lyon, INSERM U1052, CNRS UMR5286, Lyon, France. [15]Department of Neurosurgery, CHU, Dijon, France. [16]Unit of Molecular Neuro-Oncology, IRCCS Foundation, Carlo Besta Neurological Institute, Milan, Italy. [17]Service de Neurochirurgie, Hôpital Beaujon, Assistance Publique-Hôpitaux de Paris, Clichy, France. [18]Developmental Tumor Laboratory, Fundación Sant Joan de Déu, Barcelona, Spain. [19]Department of Neurosurgery, Bordeaux University Hospital. Labex TRAIL (ANR-10-LABX-57). EA 7435 – IMOTION Bordeaux University, Bordeaux, France. [20]Department of Medical Oncology, Centre GF Leclerc, Dijon, France. [21]Pediatric Neurosurgery Unit, Department of Neuroscience and Neurorehabilitation, Bambino Gesù Children's Hospital, Rome, Italy. [22]Department of Neurosurgery, Samsung Medical Center, Sungkyunkwan University School of Medicine, Seoul, Republic of Korea. [23]Department of Health Sciences and Technology, SAIHST, Sungkyunkwan University, Seoul, Republic of Korea. [24]Developmental Neurology Unit, IRCCS Foundation, Carlo Besta Neurological Institute, Milan, Italy. [25]Service de Neurochirurgie, Hôpital de la Cavale Blanche, CHRU de Brest, Université de Brest, Brest, France. [26]Department of Pathology, Hospital Sant Joan de Déu, Barcelona, Spain. [27]Central Laboratory of Pathology, Pasteur I University Hospital, Nice, France. [28]Department of Neuropathology, Sainte-Anne Hospital, Paris, France. [29]IMA-Brain, Inserm U894, Institute of Psychiatry and Neuroscience of Paris, Paris, France. [30]EA7331, Université Paris Descartes, France; Service de Génétique et Biologie Moléculaires, Hôpital Cochin, AP-HP, Paris, France. [31]Institute of Cancer and Genomic Sciences University of Birmingham Edgbaston, Birmingham, United Kingdom. [32]Department of Neurosurgery, Memorial Sloan Kettering Cancer Center, New York, NY, USA. [33]Clinical Cooperation Unit Neuropathology, German Cancer Research Center (DKFZ), Heidelberg, Germany. [34]Department of Neuropathology, Institute of Pathology, Heidelberg University Hospital, Heidelberg, Germany. [35]Division of Pediatric Neurosurgery, Seoul National University Children's Hospital, Seoul National University College of Medicine, Seoul, Republic of Korea. [36]Centre de Pathologie Et Neuropathologie Est Hospices Civils de Lyon, Lyon, France. [37]Pediatric Oncology Unit, Hospital Sant Joan de Déu, Esplugues, Barcelona, Spain. [38]Department of Pediatrics, Columbia University Medical Center, New York, NY, USA. [39]Department of Pathology and Cell Biology, Columbia University Medical Center, New York, NY, USA. [40]Department of Neurology, Columbia University Medical Center, New York, NY, USA. [41]These authors contributed equally: F. D'Angelo, M. Ceccarelli. [42]These authors jointly supervised this work: A. Lasorella, A. Iavarone. *e-mail: al2179@cumc.columbia.edu; ai2102@cumc.columbia.edu

Supplementary Figure 1

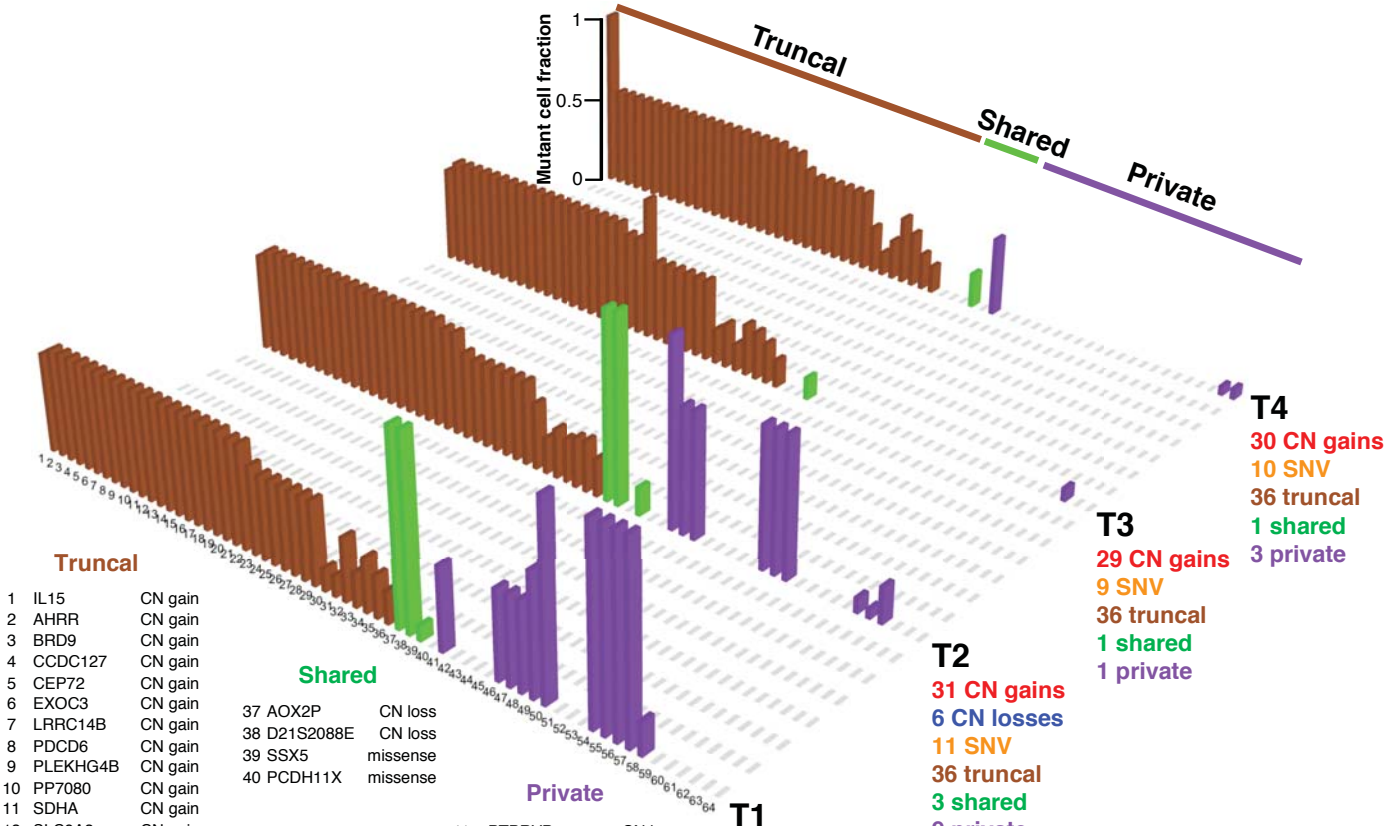

Truncal

1	IL15	CN gain
2	AHRR	CN gain
3	BRD9	CN gain
4	CCDC127	CN gain
5	CEP72	CN gain
6	EXOC3	CN gain
7	LRRC14B	CN gain
8	PDCD6	CN gain
9	PLEKHG4B	CN gain
10	PP7080	CN gain
11	SDHA	CN gain
12	SLC9A3	CN gain
13	TPPP	CN gain
14	TRIP13	CN gain
15	ZDHHC11	CN gain
16	NKD2	CN gain
17	SLC12A7	CN gain
18	SLC6A18	CN gain
19	SLC6A19	CN gain
20	TERT	CN gain
21	FGF1	CN gain
22	ARHGAP26	CN gain
23	FKBP5	CN gain
24	PDCD4	CN gain
25	BBIP1	CN gain
26	SHOC2	CN gain
27	RPL13AP6	CN gain
28	ADRA2A	CN gain
29	GPAM	CN gain
30	MANEA	missense
31	SIMC1	missense
32	DGKQ	missense
33	MYLK	missense
34	OXA1L	missense
35	SHPRH	missense
36	ZNF366	missense

Shared

37	AOX2P	CN loss
38	D21S2088E	CN loss
39	SSX5	missense
40	PCDH11X	missense

Private

41	PTPRVP	CN loss
42	CR1	CN gain
43	BZW1	CN loss
44	ZNF142	CN gain
45	BCS1L	CN gain
46	CDKN2A	CN loss
47	CDKN2B–AS1	CN loss
48	CDKN2B	CN loss
49	FLJ46361	CN loss
50	TP53I11	CN loss
51	DLEU7	CN loss
52	GUCY1B2	CN loss
53	RNASEH2B	CN loss
54	SLITRK6	CN loss
55	SLITRK5	CN loss
56	INCA1	CN gain
57	KIF1C	CN gain
58	POLR3B	splice
59	ARID4B	frameshift
60	METTL2B	missense
61	MTCH2	inframe
62	BMP6	inframe
63	MYO10	missense
64	WDR47	missense

Supplementary Figure 1 Intra-tumoral heterogeneity. Landscape of somatic alterations (SNVs and CNVs) in four regional samplings from patient #39, indicated as T1, T2, T3 and T4 on the x axis. Thirty-six somatic alterations are shared by all tumors (truncal, brown); 4 alterations are shared by 2 samples (green) and 24 lesions are found in individual samples (private, purple). The fraction of tumor cells containing the indicated lesion was estimated from VAF for SNV and absolute log R ratio for CNVs and is reported on the z axis.

Supplementary Figure 2

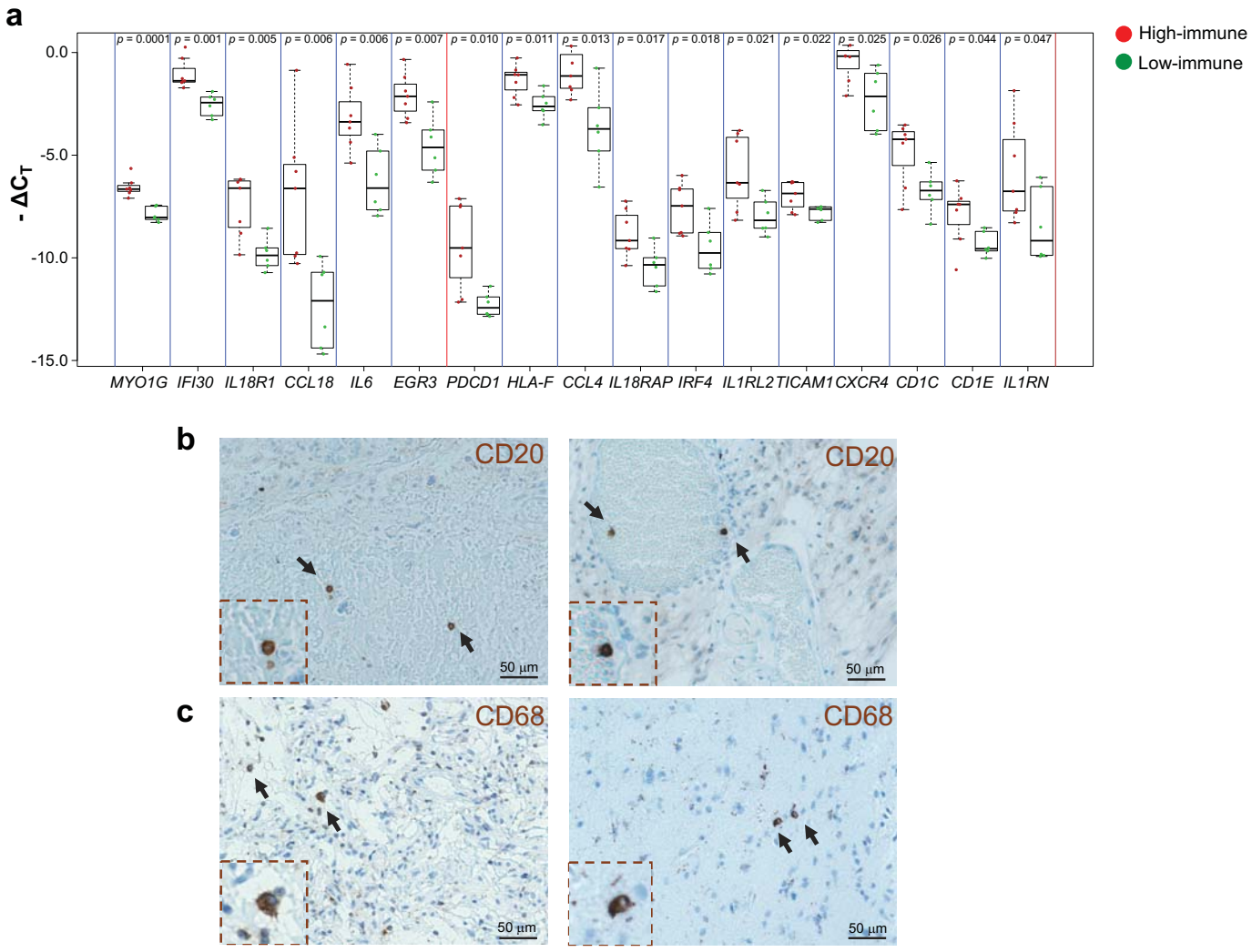

Supplementary Figure 2 Immune signature enrichment in low-grade NF1-glioma. a, RT-qPCR data of 17 immune-related genes from 14 NF1 low-grade glioma. Each point represents the mean of 3 technical replicates ($-\Delta C_T$ relative to 18S) for each sample; low-grade/low-immune glioma samples, green (n=6); low-grade/high-immune glioma samples, red (n=6); *p*-values were calculated using a two-sided t-test with Welch correction. Boxplots show median with interquartile range and minimum to maximum values. **b**, Representative microphotographs of CD20 (B cell marker) immunohistochemistry in low-grade/high-immune (left panels) and low-grade/low-immune (right panels) NF1-glioma. **c**, Representative microphotographs of CD68 (macrophage marker) immunohistochemistry in low-grade/high-immune (left panels) and low-grade/low-immune (right panels) NF1-glioma. Arrows indicate rare CD20 and CD68-positive cells. Boxed images in each panel are higher magnifications of individual positive cells. Results were validated on more than 10 independent samples to ensure the staining pattern on human tissue was reproducible.

Supplementary Figure 3

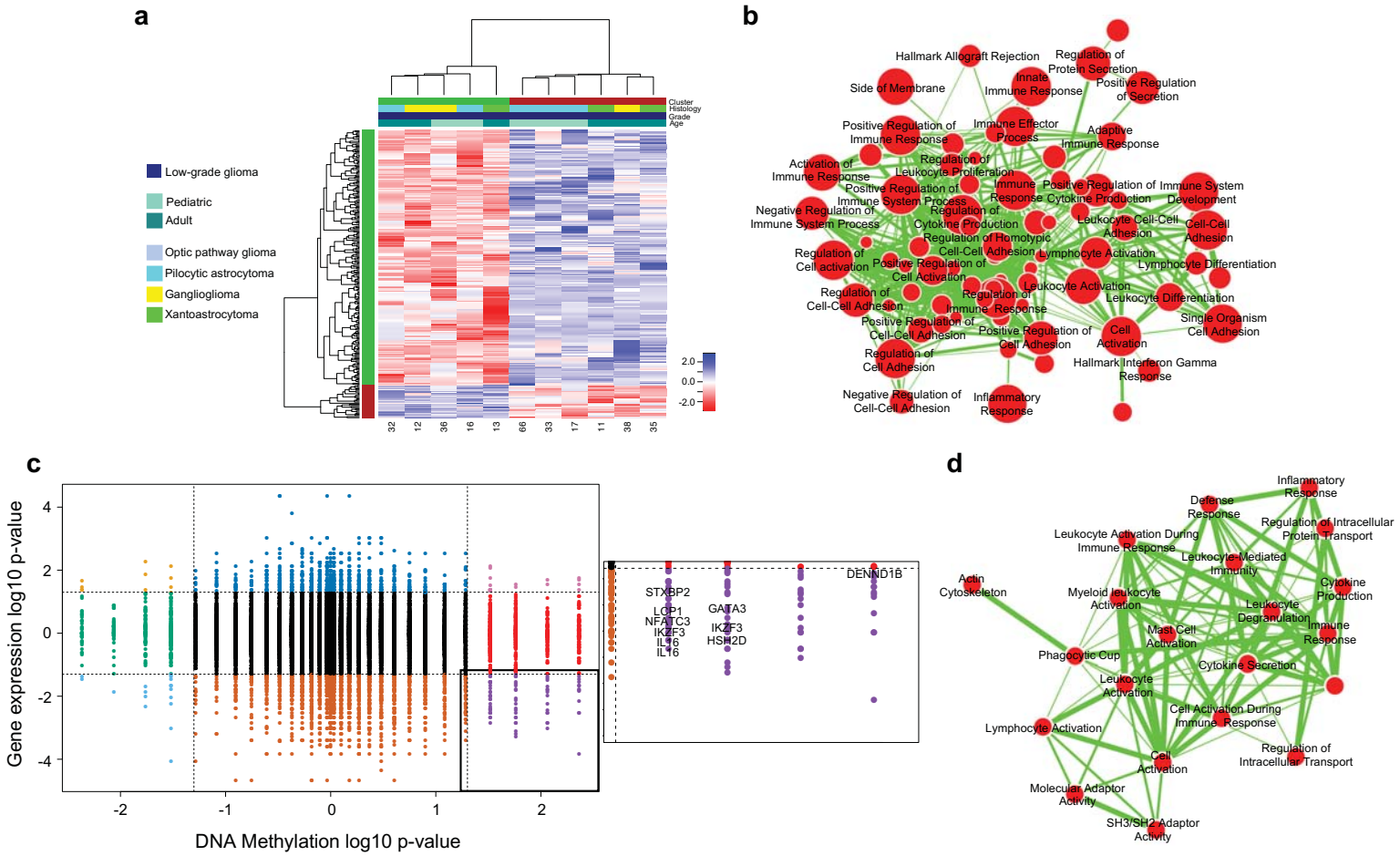

Supplementary Figure 3 Integrative analysis of gene expression and DNA methylation in low-grade NF1-glioma. a, DNA methylation hierarchical clustering of 11 low-grade glioma obtained using the Euclidean distance with Ward linkage method built on 259 probes most differentially methylated between low-grade/low-immune and low-grade/high-immune glioma samples (229 hyper- and 30 hypo-methylated probes; two-sided Mann-Whitney-Wilcoxon (MWW) test $p < 0.01$ and absolute methylation fold-change > 0.3). **b,** Enrichment map network of statistically significant GO categories in hypermethylated genes in low-grade/low-immune (n=5) versus low-grade/high-immune (n=6) glioma (two-sided MWW-GST; $q < 0.001$, normalized enrichment score, NES > 0.6). Nodes represent GO terms and lines their connectivity. Node size is proportional to number of genes in the GO category and line thickness indicates the fraction of genes shared between groups. **c,** Starburst plot (left panel) comparing DNA methylation and gene expression by RNAseq for 11,979 unique genes. For each gene, the -log10 *p*-value is plotted for DNA methylation (x axis) and gene expression (y axis). If a mean DNA methylation β-value or mean gene expression value was higher in high-immune samples (log fold-change < 0), we multiplied the -log10 *p*-value by -1. The dashed black lines indicate *p*-value at 0.05 (two-sided MWW test). The bottom right area of the plot, corresponding to the significantly hyper-methylated and down-regulated genes in low-immune compared with high-immune NF1-glioma, is magnified in the right panel and genes involved in T cell functions are indicated. **d,** Enrichment map network of statistically significant GO categories (two-sided Fisher's exact test $p < 0.001$) for the lists of down-regulated and hyper-methylated genes in low-grade/low-immune (n=5) compared with low-grade/high-immune glioma n=6). Nodes represent GO terms and lines their

connectivity. Node size is proportional to number of genes in the GO category and line thickness indicates the fraction of genes shared between groups.

Supplementary Figure 4

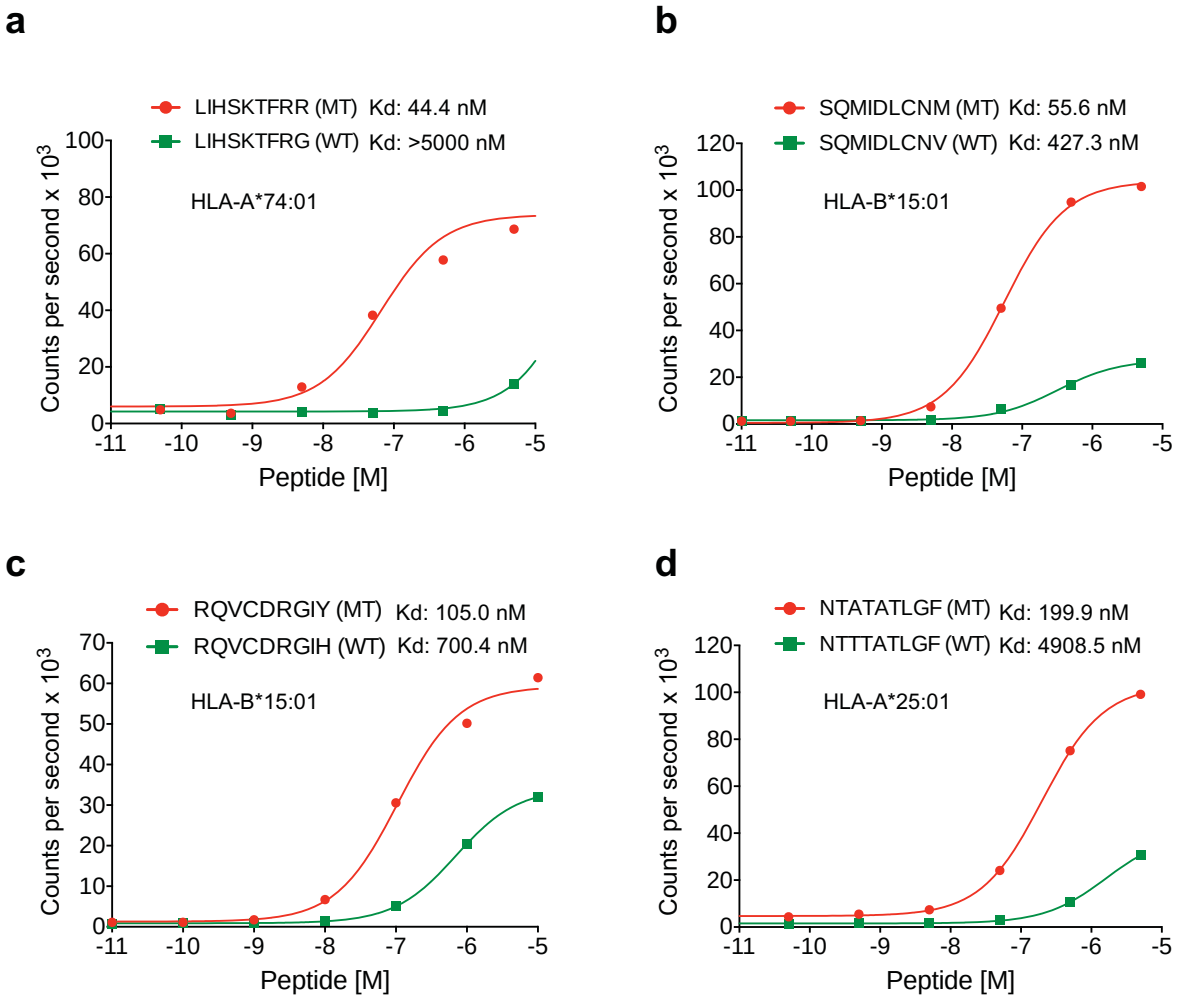

Supplementary Figure 4 Validation of predicted neoantigens in low-grade/high-immune NF1-glioma. a, *In vitro* binding affinity kinetics of neoantigens and corresponding wild type peptides for their restricted HLA class I allele. Data are shown as counts per second with increasing peptide concentration (log_{10} M). Data are mean of 2 independent experiments.

Supplementary Figure 5

a

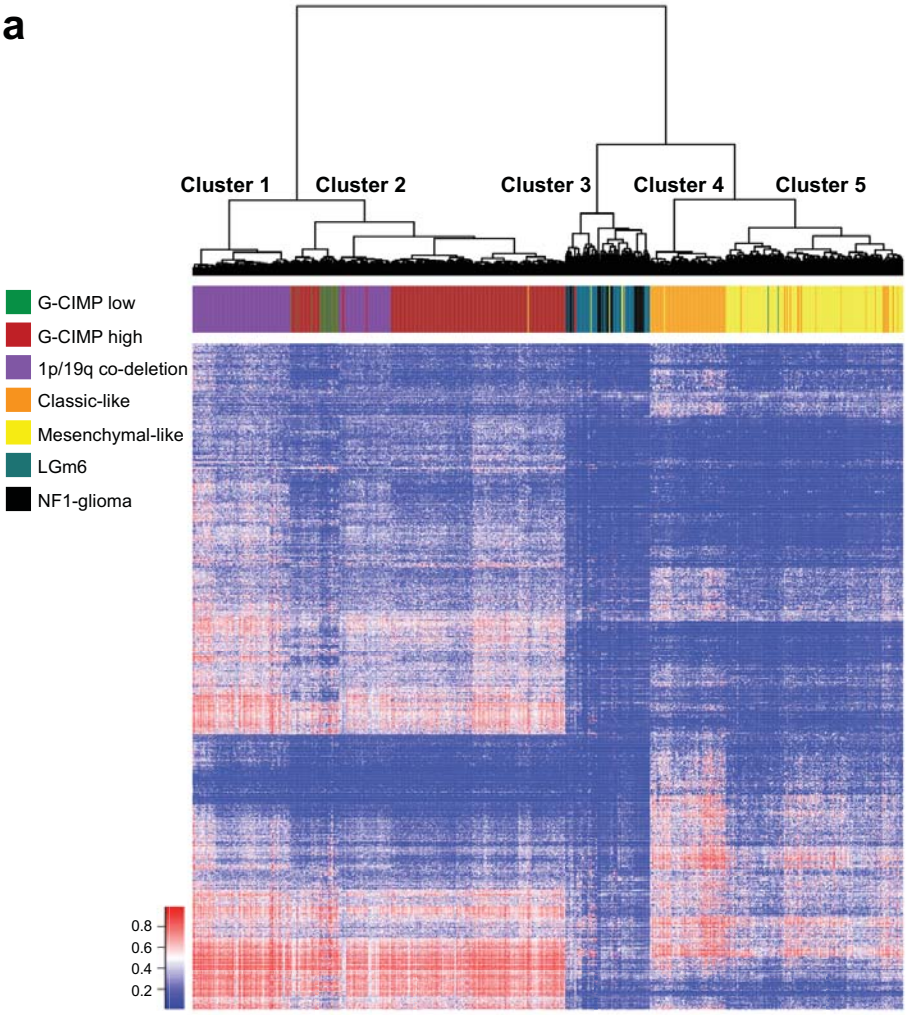

b

Cluster	G-CIMP-low	G-CIMP-high	Codel	Classic-like	Mesenchymal-like	LGm6	NF1
#1	0	0	117	0	0	0	0
#2	25	245	57	0	1	1	0
#3	3	3	0	1	4	62	**31**
#4	0	0	0	90	1	0	0
#5	0	0	0	28	182	2	0

Supplementary Figure 5 Unsupervised analysis of combined TCGA pan-glioma and NF1-glioma cohorts. a, Unsupervised analysis of DNA methylation data for TCGA pan-glioma (n=819) and NF1-glioma (n=31) cohorts according to TCGA methylation clusters. 1,233 cancer-specific DNA methylation probes were used. The dendogram identifies two main branches, one corresponding to IDH1-mutant tumors and other corresponding to IDH-wild type tumors. Cutting the dendrogram tree into five groups produced a distinct cluster (cluster 3) including 100% of the NF1 tumors (31 samples) and 95% (62 out of 65) of sporadic LGm6 tumors. **b,** Contingency table between clusters and subtypes for the dendrogram in a.

Supplementary Figure 6

a

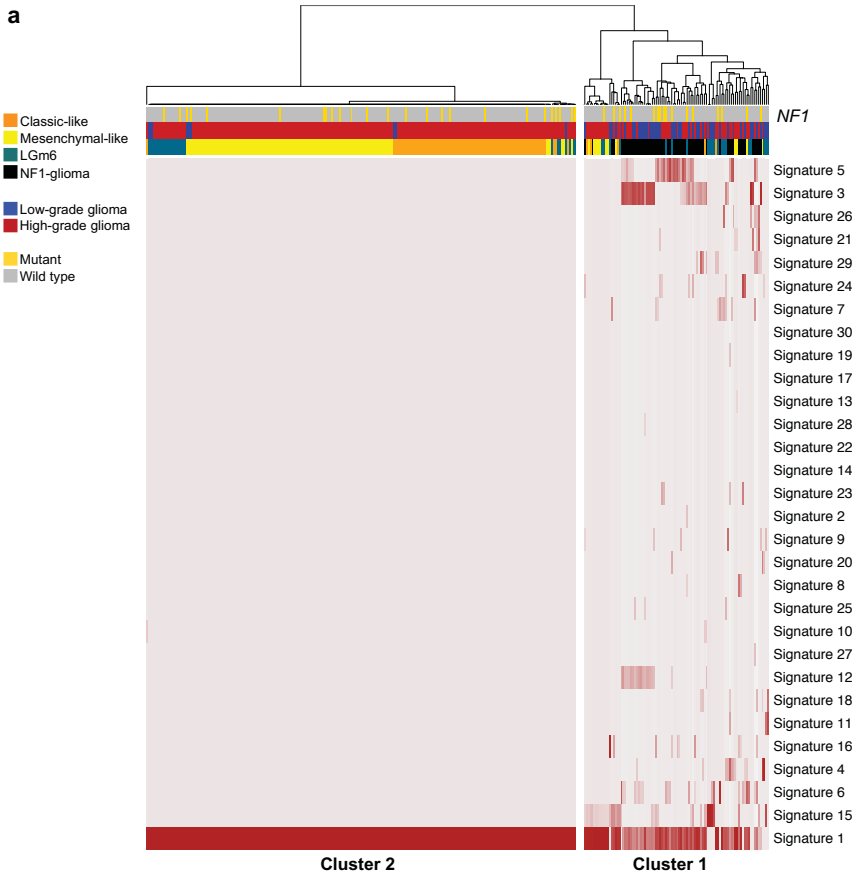

b

	Cluster 1	Cluster 2
LGm6	20	28
others	17	196

p=8.1e-08

c

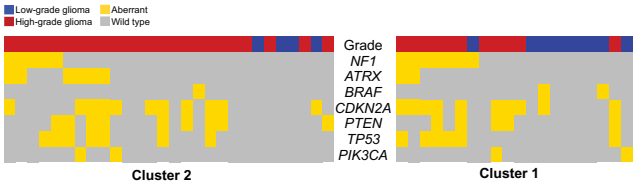

Feature	Cluster 2		Cluster 1		*p-value*
Tumor grade	High	Low	High	Low	0.02
	24/28 (86%)	4/28 (14%)	11/20 (55%)	9/20 (45%)	
NF1 mutation	5/28 (18%)		7/20 (35%)		0.2
ATRX mutation	6/28 (21%)		2/20 (10%)		0.44
BRAF mutation	1/28 (4%)		2/20 (10%)		0.56
CDKN2A loss	11/28 (39%)		10/20 (50%)		0.56
PTEN alteration	9/28 (32%)		5/20 (25%)		0.75
TP53 mutation	7/28 (25%)		6/20 (30%)		0.75
PIK3CA mutation	2/28 (7%)		2/20 (10%)		1

Supplementary Figure 6 Cancer mutation signatures of NF1-glioma and sporadic glioma. a, Heat map of the frequency of cancer mutation signatures of NF1-glioma and IDH-wild type sporadic glioma. Hierarchical clustering segregates two main groups: cluster 1 includes all NF1-glioma and cluster 2 includes the majority of sporadic glioma. **b,** Contingency table indicates the number of LGm6 and all other sporadic *IDH*-wild type glioma falling into cluster 1 and cluster 2, respectively. The significant enrichment of LGm6 glioma in cluster 1 was determined by two-sided Fisher's exact test (p=8.1e-08). **c,** Distribution of LGm6 glioma molecular features including histology grade and selected somatic genomic alterations across cluster 1 and cluster 2 (two-sided Fisher's exact test p-value is reported for each feature).